

**Numerical Simulations of Processes Contributing to Transpacific  
Transport of Asian Anthropogenic Pollution Plumes**

*Dissertation Prospectus*

Department of Atmospheric and Oceanic Science  
University of Maryland, College Park  
Advisor: Dr. Russell Dickerson  
Co-Advisor: Dr. Dale Allen

By

Elena Yegorova

9/25/2006

## Abstract

East Asian countries are going through fast economic growth and rapid urbanization at the expense of the environment. Emitted trace gases and aerosols are lofted from the planetary boundary layer (PBL) into the free troposphere (FT) through various mechanisms such as convection, frontal and orographic lifting. Once in the upper troposphere Asian pollutants are carried over the Pacific Ocean potentially impacting atmospheric chemistry and climate on an inter-hemispheric scale. Meteorological mechanisms contributing to this long-range pollutant transport can be analyzed using models and observations. The main purpose of this study is to simulate frontal passages over Eastern China and quantify Asian pollutant lofting and transport to the Pacific Ocean. I propose to use WRF/Chem: a mesoscale chemical transport model in which land surface processes, meteorology, emissions and chemistry are computed simultaneously. WRF/Chem is a relatively new chemical model which has not been widely used to run simulations over East Asia. First control runs will be done over the Northeastern U.S. for the summer of 2002 to compare WRF/Chem output with CMAQ output and measurements. Subsequently, WRF/Chem will simulate various cold front passages over Eastern China during EAST-AIRE in March-April 2005 and cold surge events over the South China Sea in December 1978 and January 1979 during WMONEX campaign and in December 2004 and 2005. Proposed work will contribute to understanding of chemical transport mechanisms responsible for Asian pollutant outflow as well as to general knowledge of the strengths and limitations of WRF/Chem simulations over Eastern Asia.

# WRF/Chem Simulations of Mechanisms Contributing to Transpacific Transport of Asian Anthropogenic Pollution Plumes

<b>1. Introduction</b>	<b>4</b>
<b>1.1. Transpacific Transport Mechanisms</b>	<b>4</b>
<b>1.1.1. Deep Convection</b>	<b>5</b>
<b>1.1.2. Fronts and the Warm Conveyor Belt</b>	<b>5</b>
<b>1.1.3. Topography</b>	<b>6</b>
<b>1.2. Meteorological Setting</b>	<b>7</b>
<b>1.3. Chemistry</b>	<b>7</b>
<b>1.4. Asian Emissions</b>	<b>8</b>
<b>1.5. Methods and Objectives</b>	<b>9</b>
<b>2. Background</b>	<b>9</b>
<b>2.1. Model Description</b>	<b>9</b>
<b>2.1.1. WRF/Chem</b>	<b>9</b>
<b>2.1.2. CMAQ</b>	<b>10</b>
<b>2.2. Emission Inventory</b>	<b>10</b>
<b>2.2.1. WRF/Chem</b>	<b>10</b>
<b>2.2.2. CMAQ</b>	<b>11</b>
<b>2.3. Observational Data</b>	<b>11</b>
<b>2.3.1. Cases selected for simulation</b>	<b>12</b>
<b>3. Preliminary Results</b>	<b>13</b>
<b>3.1. WMONEX observations</b>	<b>13</b>
<b>3.2. Evaluation of convection in MM5/CMAQ</b>	<b>15</b>
<b>3.3. WRF/Chem preliminary results</b>	<b>17</b>
<b>4. Proposed Work</b>	<b>21</b>
<b>5. Summary</b>	<b>23</b>
<b>6. References</b>	<b>23</b>

## 1. Introduction

Rapid industrialization in East Asia and especially in China has a significant impact on air quality and chemistry locally and downwind. China has one of the most rapidly growing economies in the world. While rapid economic growth has increased incomes and reduced poverty levels, environmental pollution is emerging as a major problem. Economic growth, industrialization, energy consumption, urbanization, increasing motorization, and mismanagement of natural resources add up to major air pollution problems in China. World Health Organization (WHO) reported in 2004 that out of the twenty most polluted cities in the world, sixteen are Chinese cities.<sup>1</sup> Most of China's rivers are considered polluted to some degree and half of the population has no access to clean water. The leading causes of death in China are respiratory and heart diseases many of which are related to air pollution.

China is the second-largest energy consumer in the world after the United States and the third-largest energy producer, after U.S. and Russia. Since coal makes up the bulk of China's energy consumption, China is the largest consumer and producer of coal in the world. As the Chinese economy grows so will China's coal demand. Most of China's coal is used in industrial processes, the largest single point source of urban air pollution. Sulfur dioxide and soot are the major products of coal combustion; both contribute to the formation of acid rain, which falls on about 30% of China's territory.<sup>2</sup> Vehicular emissions are another major source of air pollutants in cities. Estimates show that by 2010 in Shanghai, 75% of total NO<sub>x</sub> emissions, 94% of CO emissions, and 98% of total HC emissions will be from vehicles<sup>3</sup>.

Anthropogenic NO<sub>x</sub> emissions from Asia account for 20% of the global anthropogenic sources [Streets, et al., 2003]. Between 1975 and 1987 NO<sub>x</sub> emissions increased 65% in East Asia [Akimoto and Narita, 1994]. Furthermore a fivefold increase in NO<sub>x</sub> emissions is predicted from 1990 to 2020 [van Aardenne, et al., 1999]. In contrast, North American and European emissions of NO<sub>x</sub> are expected to decrease due to emissions controls, making Asia the most important emitter for the next 20 years.

Emissions from East Asia have been detected thousands of kilometers downwind both on the west and the east coast of North America, e.g. [Jaffe, et al., 2003]. Asian pollution plumes enhance high pollution episodes and increase "background" concentrations making it more difficult to comply with National Ambient Air Quality Standards (NAAQS). Surface ozone in the western U.S. in April-May is on average enhanced by 3-6 ppbv as a result of Asian anthropogenic emissions [Yienger, et al., 2000]. As East Asia continues to grow economically and its emissions continue to increase, there is a need to better understand mechanisms for export of Asian pollution to the global atmosphere.

### 1.1. Transpacific Transport Mechanisms

Accurate interpretation of Asian emissions and export requires a good understanding of outflow pathways and their variability on synoptic, seasonal, and interannual scales. Pollution transport from source regions occurs either in the planetary boundary layer (PBL) or in the free troposphere (FT). Pollutants travel farther at higher altitudes due to stronger upper level winds. In the PBL wind speeds

are reduced by friction with the earth's surface. In addition, a temperature inversion often isolates air in the PBL and limits its mixing with the rest of the troposphere.

Vertical transport of pollutants can be represented by eddy diffusion: mixing due to turbulent motions; species gradually move from regions of high concentration to low to reduce the gradient. If this was the sole vertical mixing method, molecules from the earth's surface would mix to 10 km in a matter of few months. More efficient transport paths exist, for instance in thunderstorms this transport time is reduced to hours. The main mechanisms responsible for lifting surface emissions into the middle and upper troposphere are deep convection, fronts and orographic forcing. These mechanisms act at different spatial and temporal scales: cloud scale and several hours for deep convection, synoptic scale and several days for fronts.

### **1.1.1. Deep Convection**

Deep convection is an important mechanism for tropospheric air transport. Rapid convective updrafts redistribute trace gases within the troposphere ([*Chatfield and Crutzen*, 1984]; [*Dickerson, et al.*, 1987]). Convection over East Asia varies seasonally, with maxima in the winter over the maritime continent and in summer over southern China. In March and April convection is restricted to Southeast Asia and enhanced by extratropical forcing from cold surge events (as discussed below). Deep convection was primarily responsible for Southeast Asian outflow observed at 7-12 km altitude at low latitudes (<35°N) during TRACE-P [*Li, et al.*, 2003]. During the spring time little rain falls over China; lofting of pollutants from the PBL by non-precipitating convection may be common over Northeast China [*Dickerson, et al.*, 2006]. Yet between February and May over East Asia, contributions of nonconvective vertical transport exceed convection [*Wild and Akimoto*, 2001].

### **1.1.2. Fronts and the Warm Conveyor Belt**

Frontal systems play an important role in the vertical redistribution of pollutants. In general, high winds associated with the passage of cold fronts clean the boundary layer and contribute to vertical mixing, thus decreasing surface concentrations. Both aircraft observations [*Bethan, et al.*, 1998] and modeling studies [*Bey, et al.*, 2001] have shown evidence of frontal lifting of pollutants from the PBL to FT. Bey et al. [2001] analyzed Asian outflow to the western Pacific in February - March, 1994 during the NASA Pacific Exploratory Mission-West (PEM-West B) mission. The authors found that frontal lifting of pollution over central and eastern China ahead of eastward moving cold fronts, followed by eastward transport in the lower FT (north of 25°N), is the principal process responsible for export of both anthropogenic and biomass burning pollution from Asia. The passage of a cold front results in an increase of CO vertical flux out of PBL, due to lifting of warm air ahead of a cold front, followed by an increased CO eastward flux to western Pacific due to rapid transport by eastward winds in the FT [*Bey, et al.*, 2001].

Asian outflow to the Pacific is strongest in spring because of frequent cyclonic activity and associated warm conveyor belts (WCBs). Transpacific transport is most efficient at this time due to prefrontal flow lifting pollutants from the surface and then southeastward-moving cold fronts transporting the pollutants above the boundary layer [*Liu, et al.*, 2003]. Ahead of cold fronts, vertical transport of PBL pollution to the FT occurs within the main ascending branch of an extratropical cyclone, i.e. the warm conveyor belt [*Cooper, et al.*, 2004]. A WCB is defined as rising streams of

warm and humid air along lines of constant entropy ahead of the cold front. WCB begins in the PBL equatorward of the cyclone, travels along and ahead of the cold front, ascending and turning anticyclonically ahead of a warm front, if present (**Figure 1**). For tracing air motion within WCB flow (for both dry and moist adiabatic processes) the wet bulb potential temperature ( $\theta_w$ ) is a conserved property [Harrold, 1973].  $\theta_w$  is attained when a parcel is brought down to 1000 mb from its lifting condensation level along a pseudoadiabat. Bethan et al. [1998] showed that ozone was lifted from the PBL to the FT by a warm conveyor belt during the development of a baroclinic wave in the North Atlantic. The authors concluded that while conveyor belts exhibit well-defined chemical signatures, several chemical tracers (such as O<sub>3</sub>, CO, NO<sub>y</sub>) and meteorological tracers (i.e.  $\theta_w$ , RH) must be measured to identify air mass differences. Lifting occurs over central and eastern China at 20°N-35°N, and the plume travels within the WCB over the western Pacific. As the system moves over the ocean, the WCB may bring in clean, marine air masses contributing to the dilution of the Asian pollution plumes (**Figure 2**). Similarly, Western Europe frequently receives outflow from North America brought over by WCB [Stohl, 2001].

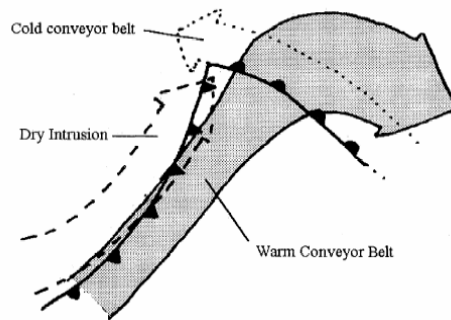


**Figure 1.** Diagram of relative isentropic flow in a midlatitude cyclone [Browning, 1990].

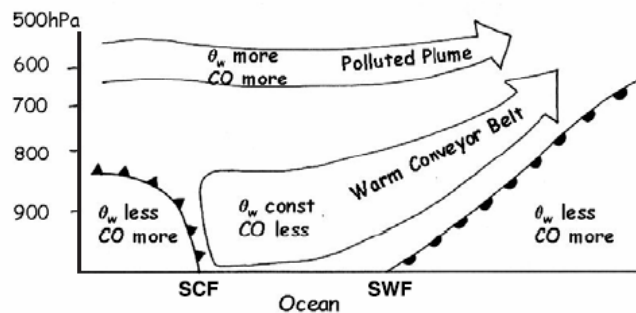


**Figure 2.** Vertical cross section of WCB. SCF – surface cold front, SWF – surface warm front. Clean WCB over the ocean splits pollution plume in the FT [Mari, et al., 2004].

Along with frontal outflow ahead of the front in the FT is the PBL continental outflow behind the front, usually capped at about 2 km altitude by strong subsidence [Liu, et al., 2003]. This plume does not travel far, fanning out over the region as the front dissipates.

### 1.1.3. Topography

Orographic lifting over central and eastern China in combination with the cold fronts provides for transport of Asian pollution to the FT [Liu, et al., 2003]. Large-scale convergence in central and eastern China was previously noted by Bey et al.

[2001], and interpreted as episodic lifting of pollution ahead of eastward moving cold fronts. Liu et al. [2003] noted convergence of polluted air around the North China Plain, along the eastern edge of mountain ranges over Southern China, and on the eastern flank of the Qinhai-Tibetan Plateau. During cold surges, northerly winds sweep anthropogenic pollutants from the North China Plain forcing the air to be orographically lifted to the FT over southern and central China. Because of orographic lifting the region of maximum vertical pollution flux (central and eastern China) differs from the region of maximum anthropogenic emissions (northern China).

## 1.2. Meteorological Setting

The meteorological mechanisms leading to long-range transport are similar over Eastern North America and over Eastern Asia. Both regions experience the passage of wave cyclones and cold fronts. Over North America, cold fronts are characterized by the collision of maritime tropical and polar continental air masses. Over North China the warmer air mass does not spend enough time over tropical waters to develop maritime characteristics. Since less moisture is advected from the ocean to the continent, Northeast China receives less precipitation in the spring.

One major difference between Eastern North America and Eastern Asia is the occurrence of monsoons. The meteorology of East Asia is controlled to a large extent by the Asian monsoon with general outflow of surface air from the continent in the winter and inflow in the summer. A monsoon is a response of the atmosphere to the differential heating between the Asian continent and the adjacent oceans. The Tibetan Plateau serves as an elevated heat source for the evolution of the Asian summer monsoon circulation. Sensible heat flux from the surface is the major source of heating on the Plateau [Yanai and Li, 1994]. A convergence zone is present over central China where air masses from the north, driven by monsoon winds, collide with maritime air masses from the south. This reflects episodic lifting of warm air ahead of eastward moving cold fronts.

The East Asian winter monsoon is characterized by “cold surges”, episodic incursion of cold midlatitude air and its penetration deep into the South China Sea. Cold surges are triggered by the extension of the Siberian anticyclone southeastward over China in connection with the passage of midlatitude synoptic waves [Ding, 1990]. They are confined to below 700 hPa and occur every 2-7 days. Cold surges enhance subtropical and tropical deep convection because of the intense low-level convergence along their leading edge [Garreaud, 2001]. Liu et al [2003] found that a La Nina year (2001) features high frequency of cold surge events and enhanced convection in Southeast Asia, while an El Nino year (1998) had a low frequency of these events and suppressed convection. In all years, Asian pollution outflow is strongest at 30°N-45°N in the BL and 20°N-35°N in the lower FT [Liu, et al., 2003]. Strong westerlies prevail at altitudes above 4 km and latitudes above 20°N [Bey, et al., 2001].

## 1.3. Chemistry

Ozone is the primary source of the hydroxyl radical (OH), which is responsible for the removal of CO, CH<sub>4</sub>, NO<sub>2</sub>, and HCs. OH is produced when O<sub>3</sub> is photolyzed by UV radiation in the presence of water vapor. The local chemical

budget of O<sub>3</sub> in the FT depends directly on vertical transport of O<sub>3</sub> from the polluted PBL or indirectly on transport of chemical precursors.

CO is destroyed by reaction with OH and produced by oxidation of isoprene and methane by OH. Tropospheric ozone is produced by photochemical oxidation of CO and volatile organic compounds (VOCs) in the presence of reactive odd nitrogen (NO<sub>x</sub>=NO+NO<sub>2</sub>). Tropospheric ozone production is limited by the supply of NO<sub>x</sub>, a product of combustion, microbial processes in soils, and lightning.

In the PBL pollutants are short-lived, if they are transported to the upper troposphere their atmospheric residence times increase. For instance, in the marine boundary layer ozone photochemical lifetime is less than a week, increasing with height to 1 month at 6 km and 1 year at 10 km [Kley, *et al.*, 1996]. Subsequently, the lifetime of lower tropospheric ozone is enhanced by the upward convective transport. On the other hand, the lifetime of upper tropospheric ozone decreases as it is transported to the lower troposphere where it is more efficiently destroyed [Lelieveld and Crutzen, 1994]. Similarly residence times for nitrogen and sulfur compounds are shortest in the PBL, where they are destroyed by surface deposition.

Marine PBL is usually low in O<sub>3</sub>, CO and NO<sub>y</sub> with high humidity. Polluted continental BL air is generally humid with high CO and HC mixing ratios, but with variable O<sub>3</sub> and NO<sub>y</sub> concentrations depending on photochemical and deposition processes.

CO is an excellent tracer for long-range transport because it is sparingly soluble in water, easily detected, measured with high precision and good temporal resolution, and has a distinct profile in the troposphere. CO is produced primarily by ground sources and destroyed throughout the troposphere, so it decreases with altitude. It is a product of incomplete combustion, with sources such as vehicles, biofuels, and biomass burning. Thus CO is a good proxy of pollution from urban, industrialized areas and biomass burning. CO has a lifetime of a few months, long enough for tracking pollution plumes on synoptic and intercontinental scales, but short enough to provide pollution enhancements in plumes relative to background. Vertical flux of CO can be used as a tracer of Asian outflow. Zonal eastward flux of Asian CO will be defined as flow through a wall located at 140°E between 20°N and 40°N.

#### **1.4. Asian Emissions**

Anthropogenic emissions include fuel combustion (both fossil and wood) and industrial activities. Anthropogenic emissions are largest in Northeastern China (in spring). Biomass burning emissions include forest fires, deforestation, savanna burning, slash-and-burn agriculture, and agricultural waste burning. Spring is the dry season in Asia, a transition between winter and summer monsoons, there is extensive biomass burning in Southeast Asia and India. The main export pathway for Asian pollution is to the Pacific in the eastward flow north of 25°N [Bey, *et al.*, 2001].

Asian chemical outflow includes contributions from other continents besides Asia. Anthropogenic emissions from Europe (18% of total CO) and biomass burning emissions from Africa (21% of total CO) contribute to the Asian outflow over western Pacific [Liu, *et al.*, 2003]. European sources are important in the lower troposphere north of 40°N, while African sources dominate in the upper troposphere at low latitudes (<35°N). The European and Asian influences are systematically mixed with the Asian pollution in the frontal outflow and do not generate distinct CO plumes. Asian biomass burning contribution to Asian outflow is maximum in March-

April, while African biomass burning and European and North American anthropogenic contributions peak in January-March [Liu, *et al.*, 2003].

## 1.5. Methods and Objectives

The present study is motivated by an ambition to capture the mechanisms of outflow of East Asian pollutants with a credible air quality model. Until recently, air quality modeling systems treated chemical processes independently of the meteorological model (“offline”), e.g. the Community Model for Air Quality (CMAQ). This approach is very attractive, requiring fewer computations. But separation of chemistry and meteorology can lead to loss of information of processes that have time scales less than the output of the meteorological model (e.g. cloud formation, rainfall, wind speed and direction). Over the past few years, several research institutes collaborated to create the Weather Research and Forecasting (WRF) model (<http://www.mmm.ucar.edu/wrf/users/document.html>). Chemical modules have been added to the WRF framework, creating an “online” WRF/Chem model (description below). Modifications to WRF/Chem continue to be implemented. This is a young model which has not yet been widely used to run simulations over Asia. Yet as WRF gradually replaces MM5, WRF/Chem will become a popular multi-scale air quality model. WRF coupled with aqueous chemistry will be used in this project to understand the effect of different transport mechanisms (i.e convection, fronts, WCB) on the types and amounts of pollutants uplifted above the PBL and available for long-range transport.

Specific objectives of the proposed work include:

1. In order to test that WRF/Chem is configured properly, compare WRF/Chem and CMAQ simulations for several ozone episodes in August 2002 over Northeast United States.
2. Configure WRF/Chem for simulations over Northeast China (i.e. use meteorology and emissions specific to East Asia).
3. Simulate conditions that were observed on the ground and by aircraft during EAST-AIRE project in April 2005 (Northeast Asia).
4. Run simulations of cold surge and convective events over South China Sea in December 2004 and January 2005 to compare current ozone concentrations to ozone levels observed by aircraft during Winter MONEX experiment in December 1978 and January 1979.
5. Investigate the strength of pollutant outflow from East Asia in relationship with vertical transport mechanisms out of the PBL.

## 2. Background

### 2.1. Model Description

#### 2.1.1. WRF/Chem

The Weather Research and Forecasting (WRF) model with online Chemistry (WRF/Chem) provides the capability to simulate chemistry and aerosols from cloud scales to regional scales. WRF/Chem has been developed by NOAA with contributions from NCAR, PNNL, EPA, and university scientists. This numerical model system is “online” in the sense that it simulates trace gases and aerosols simultaneously with meteorological fields in the WRF framework. WRF/Chem is an

extension of MM5/Chem regional-scale chemical transport model [Grell, et al., 2000] to version 2 of the nonhydrostatic WRF community model. Meteorological initial conditions and lateral boundary conditions will be taken from the NASA GEOS-4 Reanalysis. Gas phase chemistry is based upon the Regional Acid Deposition Model version 2 (RADM2) [Stockwell, et al., 1990]. Documentation for WRF/Chem can be found in Grell et al. [2005] and online at <http://ruc.fsl.noaa.gov/wrf/WG11/>.

### **2.1.2. CMAQ**

The Community Multiscale Air Quality (CMAQ) modeling system was designed to support a wide variety of modeling tasks ranging from scientific to regulatory inquiries. CMAQ can model multiple air quality subjects: tropospheric ozone, fine particulate matter, toxics, acid deposition, and visibility degradation. CMAQ modeling system incorporates output fields from emissions and meteorological modeling systems through special processors into the CMAQ Chemical Transport Model (CCTM). Then CCTM computes chemical transport modeling for multiple pollutants on multiple scales. The structure of CMAQ allows for flexibility in substituting different emissions processing systems and meteorological models. Yet the model is “offline”, since meteorology fields are computed separately from the chemistry. Meteorological variables are taken from the National Center for Atmospheric Research/Pennsylvania State University Mesoscale Model 5 (MM5). The MM5 simulations are performed with a modified Blackadar planetary boundary layer scheme and a standard nudging process [Zhang and Zheng, 2004]. Documentation for CMAQ is available at <http://www.epa.gov/asmdnerl/CMAQ/CMAQscienceDoc.html>.

## **2.2. Emission Inventory**

### **2.2.1. WRF/Chem**

North American WRF/Chem anthropogenic emissions inventory is based upon the U.S. EPA's 1999 National Emissions Inventory (NEI99, version 3) released November 2003 and updated with any changes prior to March 2004. NEI99 inventory includes emissions of 7 primary species (NO<sub>x</sub>, VOC, CO, SO<sub>2</sub>, NH<sub>3</sub>, PM<sub>2.5</sub> and PM<sub>10</sub>), 41 speciated VOC compounds, and 5 PM<sub>2.5</sub> aerosol species, and are divided into 24 average hourly emissions. All biogenic sources of NO<sub>x</sub>, VOC, and all fire-related emissions have been removed from this inventory. Area and mobile source emissions are distributed on a 4 km horizontal resolution Lambert-Conformal grid encompassing continental United States, southern Canada, and northern Mexico (24–52°N latitude, 60–125°W longitude). The 4 km horizontal data spacing of the area emissions allows for high spatial resolution. Point emissions are given in terms of latitude and longitude location, with stack parameter information included for plume-rise calculations. While processed emissions are output for each hour of an ozone season day (OSD), emissions for specific days of the week or months are unavailable. Also the effect of temperature on emissions is not included in the processed inventory since this requires coupling between the emission data and meteorological fields. Instead, NEI99 emissions are based on climatological average temperatures. NEI99 reference is available at <http://ruc.fsl.noaa.gov/wrf/WG11/anthropogenic.htm>. In addition, an Emission Inventory Map viewer (<http://map.ngdc.noaa.gov/website/al/emissions>) is provided for visualization of

processed emissions and quantification of gridded emissions within any latitude-longitude box.

Emissions for East Asia will be taken from the inventory of Asian emissions in 2000 developed for atmospheric modeling of TRACE-P and ACE-Asia experiments [Streets, *et al.*, 2003]. Gridded emissions are available at several spatial resolutions ranging from 1°x1° to 30 s x 30 s (available at [http://www.cgrer.uiowa.edu/EMISSION\\_DATA/index\\_16.htm](http://www.cgrer.uiowa.edu/EMISSION_DATA/index_16.htm)). The domain is bounded by Pakistan in the West, Japan in the East, Indonesia in the South and Mongolia in the North. Emissions are available for nine major chemical species: NO<sub>x</sub>, CO<sub>2</sub>, CO, SO<sub>2</sub>, CH<sub>4</sub>, NH<sub>3</sub>, black carbon aerosol (BC), organic carbon aerosol (OC), and nonmethane volatile organic compounds (NMVOC), where NMVOC are speciated into 19 categories. Only anthropogenic emissions are included in the inventory. Annual emissions are subcategorized as daily and monthly emissions due to considerable seasonal variation for some species.

### 2.2.2. CMAQ

The Sparse Matrix Operator Kernel Emissions (SMOKE) is used to convert emission inventory data into formatted emission files required by CMAQ. SMOKE processes data from 2002 emissions inventories that were compiled by several regional planning organizations, all based on NEI2002 inventory. Midwest emissions are taken from Midwest Regional Planning Organization (MWRPO) inventory, Southeast emissions are from Visibility Improvement State and Trail Association of the Southeast (VISTAS) inventory, and Northeast emissions are from The Mid-Atlantic/ Northeast Visibility Union (MANE-VU) inventory. CMAQ ready emission files contain both anthropogenic and biogenic sources.

### 2.3. Observational Data

The data to be used in the proposed project will be drawn from several field experiments as well as modeling studies. A U.S.-China joint Intensive Field Campaign (IFC) in February-April 2005 was carried out under the sponsorship of EAST-AIRE (East Asian Study of Tropospheric Aerosols: an International Regional Experiment). During this field campaign in-situ measurements of trace gases and aerosols were collected both at ground stations and aboard an aircraft (**Figure 3a**). Ground based station at Xianghe provides observations of O<sub>3</sub>, CO, CO<sub>2</sub>, SO<sub>2</sub>, NO, NO<sub>y</sub> as well as aerosol optical properties in March 2005. Aircraft measurements were collected in April 2005 based out of Shenyang, the capital of the Liaoning province in Northeast China, about 650 km Northeast of Beijing [Dickerson, *et al.*, 2006]. Eight flight missions were performed throughout April 2005 under various weather conditions. Observations of trace gases (CO, O<sub>3</sub>, SO<sub>2</sub>) and aerosol properties as well as flight routes are available at [http://www.atmos.umd.edu/~yuan/web\\_proj/station.htm](http://www.atmos.umd.edu/~yuan/web_proj/station.htm).

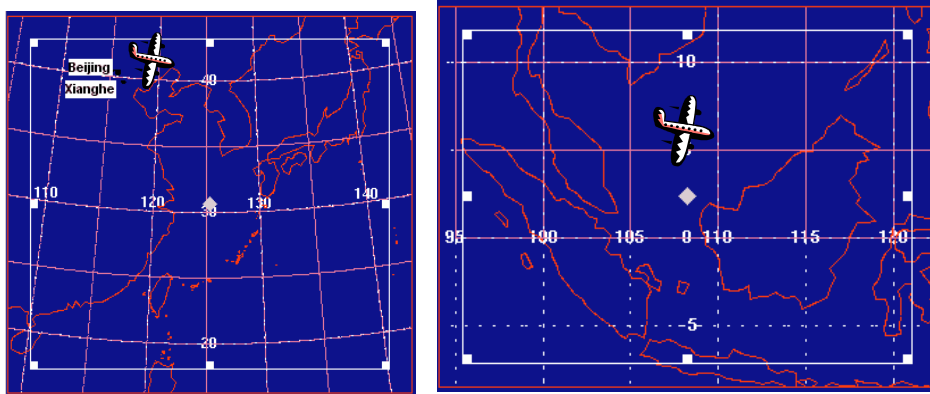


**Figure 3.** a) Simulation map for NE Asia with locations of the observation site at Xianghe and the EAST-AIRE flight. b) Simulation map of South China Sea and approximate location of WMONEX flights.

The proposed project will also use observational data measured onboard the NCAR Electra aircraft during the Winter Monsoon Experiment (WMONEX) based in Malaysia between November 17, 1978 and January 9, 1979. This campaign included flights over the Pacific Ocean and South China Sea (**Figure 3b**). A number of variables were measured from the NCAR Electra as it flew over the Western Pacific; the ozone data were never analyzed or published prior to this study. Flight tracks, profiles and time series are available at <http://www.atmos.umd.edu/~elena/monex.htm>.

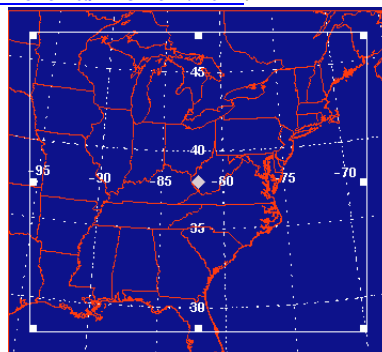


**Figure 3.** c) Simulation map of Northeast U.S.

WRF/Chem performance on the Northeast U.S. grid (**Figure 3c**) will be analyzed using previous CMAQ 2002 runs done by the Regional Atmospheric Measurement, Modeling and Prediction Program (RAMMPP) and summaries of the Operational Air Quality Forecasting for Mid Atlantic Region performed at University of Maryland, College Park ([http://www.atmos.umd.edu/~forecaster/summary\\_2002.htm](http://www.atmos.umd.edu/~forecaster/summary_2002.htm)).

### 2.3.1. Cases selected for simulation

During EAST-AIRE mission five cold front passages were identified: on March 5, March 10, March 16, March 19, and March 21 (available at <http://abc-gosan.snu.ac.kr/sfc.html>). These cold front passages were characterized by abrupt wind shifts (from south to west or northwest), increases in atmospheric pressure, and decreases in temperature and relative humidity [Li, *et al.*, 2006]. Ground observations from the Xianghe station are available for these episodes. Aerosol loading, NO<sub>y</sub>, SO<sub>2</sub>,

and CO accumulated before the passage of a cold front and quickly decreased after the cold front passage.

On April 5, 2005 the Y-12 research aircraft of the EAST-AIRE project flew ahead of a cold front. On this day the aircraft flew from Shenyang, located in China's industrial region with a population over six million. A cold front was moving from the south northeastward, sweeping out most populated and polluted regions of China within the warm sector ahead of the cold front. Concentrations of O<sub>3</sub>, CO, SO<sub>2</sub> and aerosols peaked just above the inversion at about 1 km altitude, and then fell off sharply to levels still above the background. This system brought little moisture to the region of observation and few clouds were observed. According to the back trajectories low level flow was from the Southwest and upper level flow was from the West. Dickerson et al. [2006] concluded that neither pre-frontal zone convection nor a WCB were responsible for lofting the pollutants out of the BL in this event. This episode is an example of long-range transport of significant concentrations of particulate matter, lofted upward by a small convective system 27 hours prior to observations. Since little to no precipitation was observed during this event, dry convection was introduced as a very effective method of vertical transport of pollutants.

On April 7, 2005 a similar flight was carried out as part of EAST-AIRE. As the cold front moved out, a continental polar air mass brought cool, dry air to the Shenyang region. Aircraft measured SO<sub>2</sub> and CO levels were low, but ozone and aerosol loading was high around 2.5 km altitude. Back-trajectories at all levels originate in the Northwest, a sparsely populated region of Mongolia. Dickerson et al. [2006] concluded that high winds in the high pressure area lofted dust from the Gobi desert and subsidence brought ozone rich air from the upper troposphere/lower stratosphere region to the middle troposphere.

On December 28 and 29, 1978 a rapid-moving cold surge moved off the coast of South China and spread southward. Convective activity increased in the central part of the South China Sea and cyclonic circulation intensified in the region of the December 29 flight. Although the average background ozone for this flight was around 25 ppb, significant signal increases were noted throughout the flight. Ozone mixing ratio spikes of 40-55 ppb were observed during this flight and are postulated to correspond to subsiding ozone-rich upper tropospheric air, transporting ozone downward. More cold surge episodes were documented during WMONEX flights: on December 10-11, 14-18, 19-24, and 28-30.

Several high ozone episodes occurred during the summer of 2002. The proposed study will model several of the following episodes: July 1-3, July 17-19, July 22-23, and July 31-August 5. During all of these episodes there is a center of high pressure somewhere over the Mid Atlantic region. The high temperatures, low cloudiness, and calm wind conditions contribute to efficient photochemical production of ozone and its build up over the region. Ozone during the July 17-19 episode is enhanced by the presence of the Appalachian lee trough, which brings ozone precursors from the south. An ozone code orange or code red is issued during all of these episodes. The ozone events end as a cold front system pushes through the region, ventilating the PBL and enhancing vertical mixing.

### **3. Preliminary Results**

#### **3.1. WMONEX observations**

WMONEX campaign included flights over the Pacific Ocean and South China Sea. Total number of minutes of observations is shown in **Figure 3**. **Figure 4** is a plot of average ozone mixing ratios over the South China during WMONEX. The tropical, marine lower troposphere is characterized by low ozone concentrations; here averaged 25-30 ppb. The ozone mixing ratio measurements taken during the WMONEX 1978 mission provide a benchmark to test for trends in the composition of the atmosphere, and thus climate forcing, over the western Pacific – an area surrounded by countries that have been developing rapidly in the intervening decades. Since no field campaigns have examined the chemical composition of air over the South China Sea since WMONEX, direct comparison of these observations to more recent data is impossible. Thus modeling the WMONEX observational region at a more recent time will provide a basis of comparison 1978-1979 ozone levels to 2004-2005 levels. The 2004-2005 period has been preliminary selected since it is the most recent time period with similar Multivariate ENSO Index (MEI) as WMONEX period (available at <http://www.cdc.noaa.gov/people/klaus.wolter/MEI/table.html>).

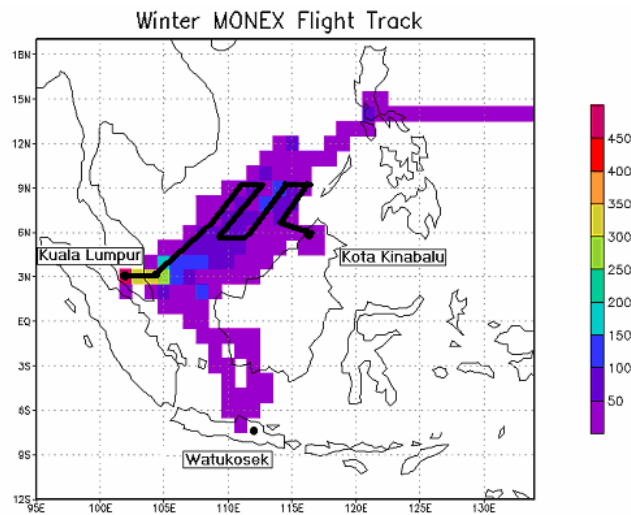


**Figure 3.** Collection of available measurements for all WMONEX flights. Scale: minutes within 1° x 1° grid. The bold black line depicts the December 29, 1978 flight track when several cloud rings were penetrated.

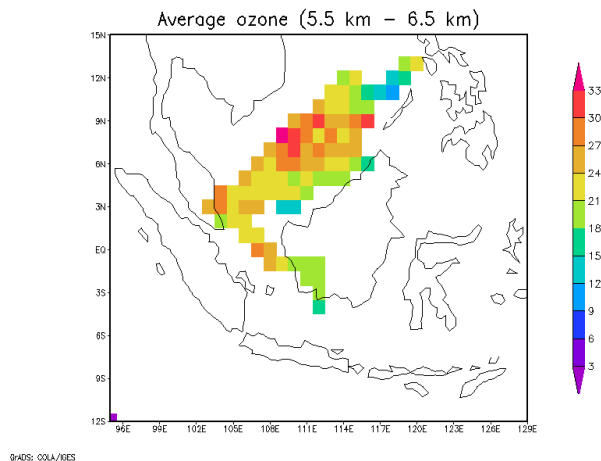


**Figure 4.** Average ozone concentrations (ppb) over the South China Sea measured at cruise altitude 5.5 km – 6.5 km.

A Dasibi ultraviolet absorption sensor monitored ozone mixing ratios during WMONEX. Although the average background ozone for December 29, 1978 flight was around 25 ppb, ozone peaked above 40-50 ppb throughout the flight (**Figure 5**). The marine boundary layer is characterized by a local maximum in H<sub>2</sub>O and sea-salt Br, and undergoes rapid photochemical destruction of ozone. The observed ozone signal jumps are hypothesized to correspond to so-called cloud rings, which were visually identified during the December 29, 1978 flight by observers on the aircraft and later from time-lapse 16 mm films. Cloud rings or open cell circulation has downward motion and clear sky in the center, and is surrounded by cloud associated with upward motion. The subsiding air channel within the cloud ring's clear region transports upper tropospheric ozone-rich air into the lower levels where ozone's lifetime is shorter. These measurements demonstrate how convective mixing, can lead to vertical transport and destruction of ozone over remote, tropical, marine environments.

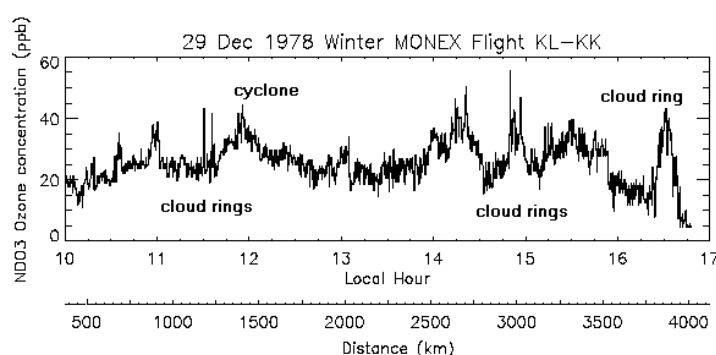


**Figure 5.** Ozone mixing ratio series with respect to distance and local time for part of the December 29, 1978 flight. Distance is measured as traversed flight path from Kuala Lumpur. Flight start time 00:41 UTC (8:41 LST) and end time 8:48 UTC (16:48 LST). Flight altitude was nearly constant at ~6 km until descent for landing, starting at 16:20 LST, 3810 km from Kuala Lumpur. Largest cloud ring is about 50-100 km in diameter, smallest are about 10 km.

### 3.2. Evaluation of convection in MM5/CMAQ

The timing and location of convection can determine when and where maximum pollutant concentrations are observed. How realistically a regional-scale or a multi-scale chemical transport model depicts an air pollution event or its transport depends on meteorological fields used in the model. CMAQ incorporates meteorological output fields from MM5 modeling system. Thus how well CMAQ simulates vertical uplift of pollution during convective events depends on how well MM5 captures convective events in comparison with observations. A verification of short-range numerical model forecasts of warm season convection was conducted over two U.S. regions: Northeast and Midwest. All available days from the summer 2002 were evaluated using accumulated precipitation products from the NCEP hourly, multi-sensor National Precipitation Analysis (NCEP NPA) and the fifth-generation Pennsylvania State University–National Center for Atmospheric Research Mesoscale Model (MM5) with Modified Blackadar PBL scheme and Kain–Fritsch convective parameterization. Area averages over two 500 km<sup>2</sup> regions show good agreement between model forecast and observations with an average R<sup>2</sup> value of 0.76. The square of the correlation coefficient decreases to 0.42 as the area of comparison is gradually decreased to a 16 km<sup>2</sup> region. Analysis of the diurnal cycle of model and observed accumulated precipitation showed that MM5 peak precipitation is on

average 2-3 hours earlier and 25% - 42% greater in magnitude than NCEP NPA (Figure 6). Overall MM5 correctly forecasts large-scale convective events, but time lag in the peak precipitation might be problematic for air quality modeling.

Verification of convective occurrence was based on contingency table (Table 1) in which each element of the table equals the number of occurrences in which CMAQ and NCEP did or did not report precipitation over a 24 hour period [Wilks, 1995]. The canonical threat score is a measure of the fractional overlap between the observed and model areas meeting or exceeding a specified precipitation threshold

(here 1.25 mm): 
$$TS = \frac{a}{a+b+c}$$

		Observed	
		Yes	No
Forecast	Yes	a	b
	No	c	d

Table 1. A 2x2 contingency table. Shaded boxes are correct forecasts.

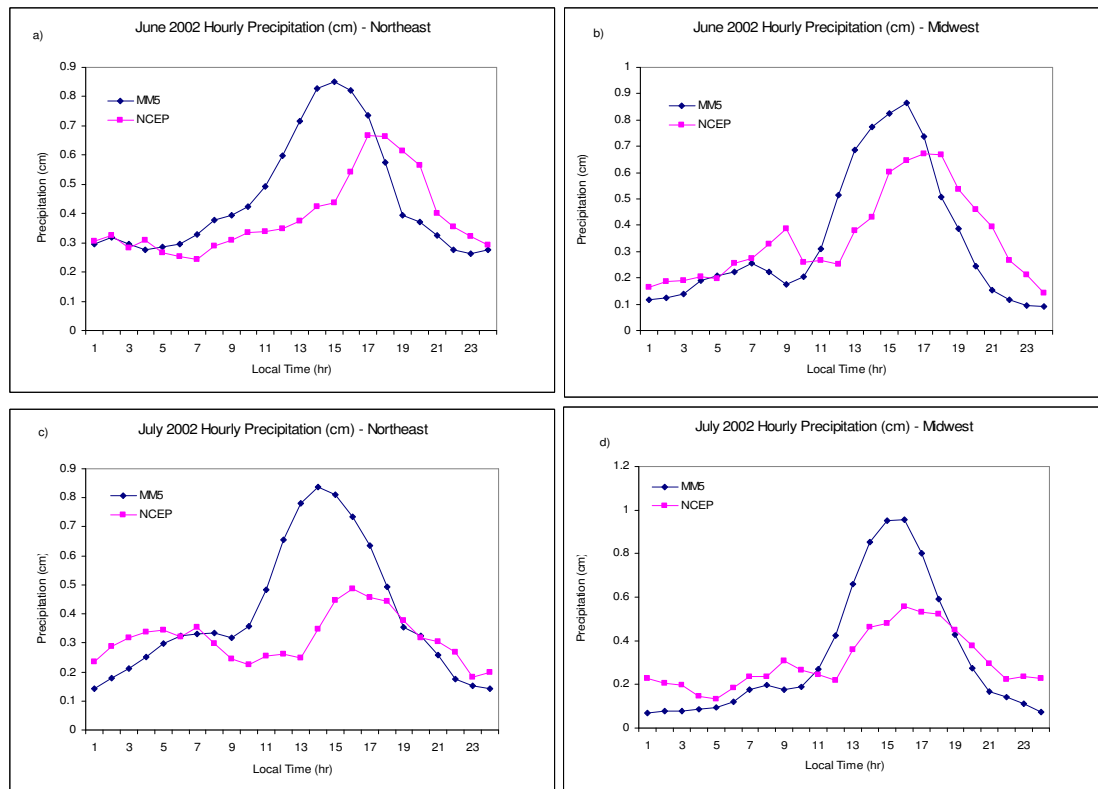


Figure 6. Total hourly precipitation for June and July 2002 in the two 500 km<sup>2</sup> regions: Northeast and Midwest.

Contingency forecasts of the area coverage of the 24-h accumulated precipitation in convective events show skill comparable to the lower-resolution, operational models (Table 2), with median threat scores of 0.358 and 0.326 for all modes of convection (defined as linear, multicellular, or isolated) for Northeast and Midwest respectively. The definitions for the convection modes are as follows: *linear convection* - length to width ratio of at least 3:1, persists for at least 3 hours, and has an areal coverage of at least 500 km<sup>2</sup>; *multicellular convection* - length:width ratio

less than 3:1, persists for at least 3 hours and has an areal coverage of at least 500 km<sup>2</sup>, *isolated convection* - spatial coverage of less than 500 km<sup>2</sup>. Analysis was performed only for days when convection occurred. When calculated by convective mode, threat scores are highest for most organized modes with largest spatial scale – linear (0.721, 0.533) and multicellular (0.55, 0.344), and the lowest for small scale isolated events (0.171, 0.134). Threat scores are comparable with published results for operational models.

Percentile	Threat Score (Threshold = 1.25 mm)	
	Northeast (43 days)	Midwest (43 days)
<i>All Convection</i>		
25th	0.171	0.180
50th	0.358	0.326
75th	0.636	0.466
<i>Linear</i>	Northeast (5 days)	Midwest (7 days)
25th	0.638	0.438
50th	0.721	0.533
75th	0.818	0.674
<i>Multicellular</i>	Northeast (20 days)	Midwest (25 days)
25th	0.333	0.250
50th	0.550	0.344
75th	0.678	0.434
<i>Isolated</i>	Northeast (18 days)	Midwest (11 days)
25th	0.124	0.109
50th	0.171	0.134
75th	0.288	0.200

**Table 2.** Threat scores calculated by type of convection (all, linear, multicellular, isolated) and by region (Northeast, Midwest).

Overall MM5 and NCEP Stage II observations show good agreement. The limiting resolution for agreement is variable from 5°x5° to 1°x1°. MM5 shows stronger peak precipitation a few hours before actually observed in NCEP NPA. This time lag in diurnal cycle should be considered when analyzing CMAQ simulations.

### 3.3. WRF/Chem preliminary results

The 1999 NEI emissions used in WRF/Chem (hereafter referred to as WRF/Chem) and the 2002 NEI regional emissions used in CMAQ (hereafter referred to as CMAQ) were analyzed for June. In preparation for running WRF/Chem, 1999 NEI emission files are extrapolated to fit on the selected grid, adjusted based on initial and boundary conditions and output as a netCDF file containing 24 hourly values on a WRF/Chem grid (for random test date June 20, 2006). The 2002 NEI emissions from several regions are processed outside the department by SMOKE and output as daily netCDF files with hourly values.

For the comparison June monthly average values are used for CMAQ and 24 hour total values for WRF/Chem for June 20, 2006. Both domains include Northeast and Midwest U.S. CMAQ has 172 longitudes, 172 longitudes, and 16 vertical layers, and WRF/Chem emissions were processed to match CMAQ vertical and horizontal domain. Only emissions that had a 1:1 speciation correspondence between CB4 mechanism used in CMAQ and RADM2 mechanism used in WRF/Chem were compared: CO, NO<sub>x</sub>, SO<sub>2</sub>, NH<sub>3</sub>, CH<sub>2</sub>O (formaldehyde), C<sub>3</sub>H<sub>8</sub> (isoprene), and C<sub>2</sub>H<sub>6</sub>

(ethane). Column total emissions were summed and compared for the total domain (30°N - 47°N, 94°W-67°W), Ohio State (38.2°N – 42.1°N, 84.9°W-80.3°W), then one of most polluting power plants in Conesville, OH (40.25°N, 81.87°W), and finally for Wisconsin State (42.3°N -47°N, 92.9°W-86.3°W) (**Table 3**).

For the total domain CO, NO<sub>x</sub>, SO<sub>2</sub>, and NH<sub>3</sub> values are very similar in WRF/Chem and CMAQ. CO, NO<sub>x</sub>, SO<sub>2</sub> WRF values exceed CMAQ values for all domains, perhaps due to some policy related emissions reductions included in the 2002 NEI. NH<sub>3</sub> totals are slightly higher for CMAQ. Larger differences are seen in formaldehyde, isoprene, and ethane, with CMAQ values exceeding WRF/Chem. Since biogenic emissions are calculated online in WRF/Chem, here anthropogenic WRF/Chem emissions are compared to combined anthropogenic and biogenic CMAQ emissions. The large difference in isoprene is a good indicator of biogenic signature in CMAQ emissions. Decreasing the domain size from total domain to state domain to city domain, decreases emission totals, as to be expected. Comparing Ohio and Wisconsin, while Wisconsin is larger by area, Ohio emissions are higher for all species. Interestingly, SO<sub>2</sub> emissions at a power plant in Conesville, OH exceed SO<sub>2</sub> emissions for all of Wisconsin state in both WRF and CMAQ. Total domain emissions for CO look very similar for WRF and CMAQ (**Figure 7**); difference plot between WRF and CMAQ shows regions of disagreement (**Figure 8**).

	Total Domain			Ohio State			Conesville,OH			Wisconsin State		
	WRF	CMAQ	WRF-CMAQ	WRF	CMAQ	WRF-CMAQ	WRF	CMAQ	WRF-CMAQ	WRF	CMAQ	WRF-CMAQ
CO (Gg C/day)	158.7	155.	3.72	13.81	12.39	1.42	2.92	2.42	0.5	7.5	6.76	0.74
NO <sub>x</sub> (Gg NOx/day)	36.1	32.9	3.22	4.13	3.69	0.44	0.77	0.6	0.17	1.69	1.54	0.15
SO <sub>2</sub> (Gg S/day)	33.3	29.2	4.09	6.2	5.37	0.83	1.72	1.05	0.67	1.17	0.93	0.24
NH <sub>3</sub> (Gg N/day)	6.14	6.36	-0.22	0.32	0.65	-0.33	0.08	0.1	-0.02	0.57	0.53	0.04
Formaldehyde (Gg C/day)	0.13	0.65	-0.52	0.01	0.04	-0.03	0.002	0.008	-0.006	0.006	0.043	-0.037
Isoprene (Gg C/day)	0.01	54.12	-54.11	1.17E-03	2.08	-2.08	2E-04	0.44	-0.44	6E-04	2.92	-2.92
Ethane (Gg C/day)	0.34	1.91	-1.58	0.03	0.1	-0.07	0.005	0.022	-0.017	0.016	0.114	-0.098

**Table 3.** WRF and CMAQ emission totals calculated for total domain, Ohio State, Conesville, OH, and Wisconsin State; differences are shaded.

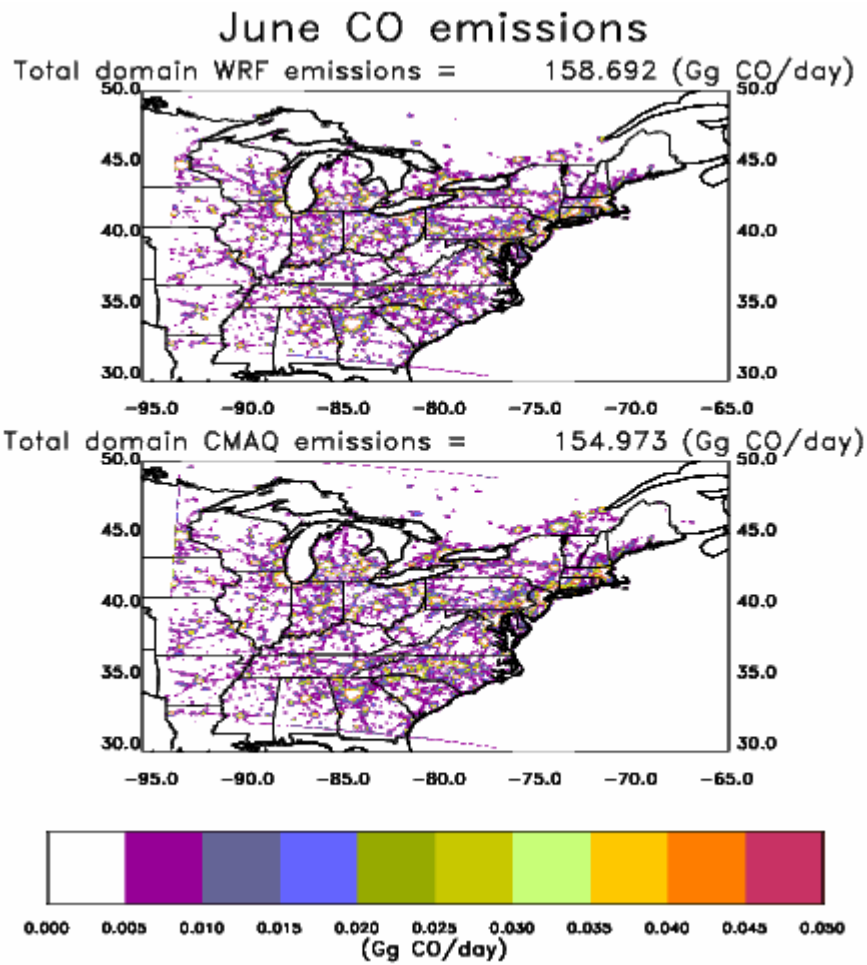


Figure 7. CO total domain emissions for WRF and CMAQ.

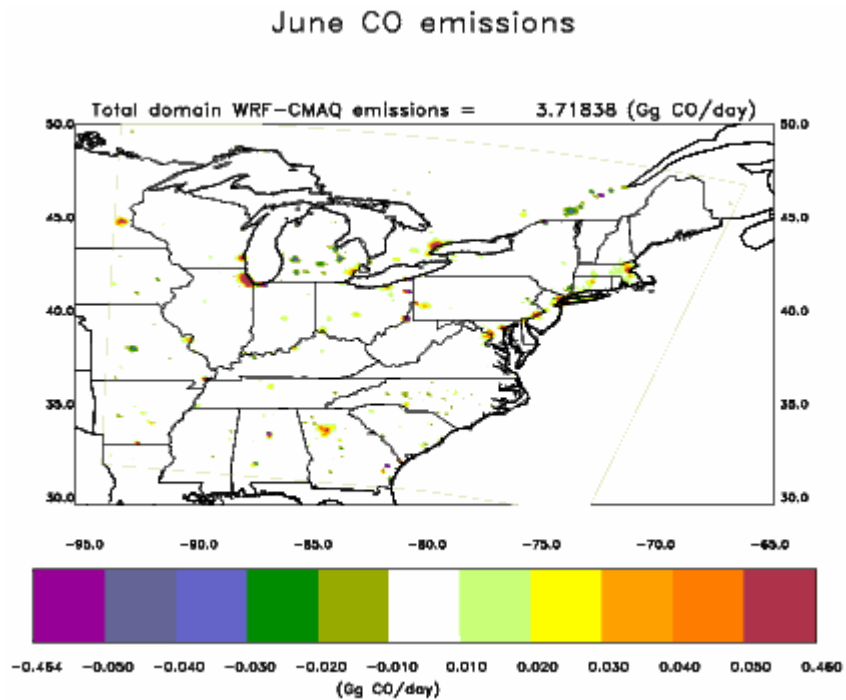
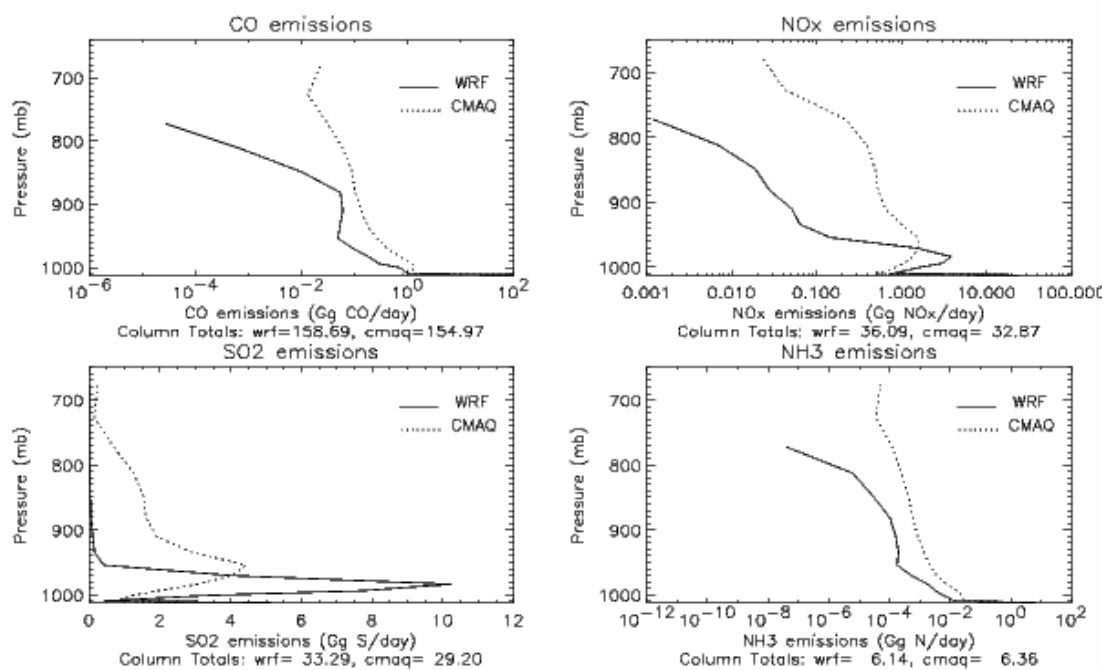


Figure 8. CO total domain emissions difference plot between WRF and CMAQ.

Vertical profiles were plotted for emissions summed over the above mentioned domains. Vertical profiles for the total domain are shown in **Figure 9** and in tabular form are summarized in **Table 4**. For all species WRF exceeds CMAQ for the lowest several layers, but for the rest of the profile CMAQ values are greater. For NO<sub>x</sub> and SO<sub>2</sub> WRF places a sharp peak around 980 mb with values dropping off rapidly with height.

### Total Domain Vertical Profiles



### Total Domain Vertical Profiles

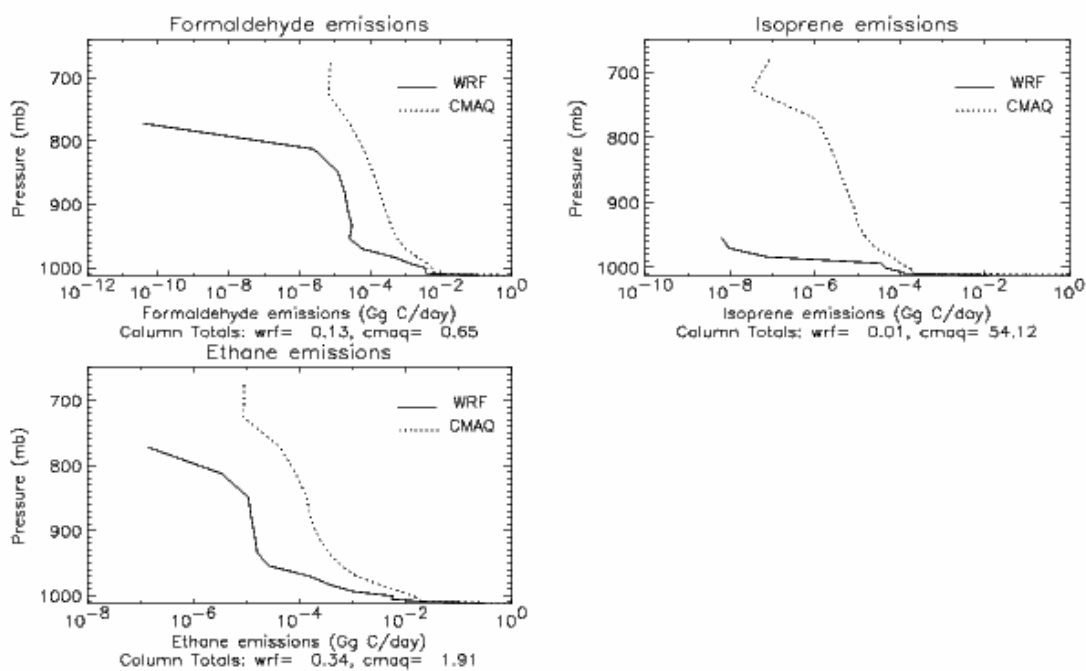


**Figure 9.** Total domain vertical profiles of emissions WRF (solid line) and CMAQ (dashed line).

Pressure (mb)	CO (Gg CO/day)			NO <sub>x</sub> (Gg N/day)			SO <sub>2</sub> (Gg S/day)			NH <sub>3</sub> (Gg N/day)		
	WRF	CMAQ	WRF-CMAQ	WRF	CMAQ	WRF-CMAQ	WRF	CMAQ	WRF-CMAQ	WRF	CMAQ	WRF-CMAQ
1011	155	148	6.79	24	22	1.99	5.11	2.64	2.47	6.1	6.25	-0.15
1008	1.06	0.786	0.274	0.812	0.48	0.332	0.445	0.757	-0.312	1.24E-02	2.90E-02	-1.66E-02
1003	0.875	1.11	-0.235	1.08	0.646	0.434	1.65	0.884	0.766	1.06E-02	2.68E-02	-1.62E-02
997	0.743	1.39	-0.647	1.53	0.819	0.711	3.36	1.22	2.14	5.83E-03	2.41E-02	-1.83E-02
989	0.289	1.22	-0.931	3.03	1.08	1.95	7.71	1.96	5.75	3.31E-03	1.64E-02	-1.31E-02
977	0.189	0.748	-0.559	3.8	1.35	2.45	10.2	3.05	7.15	1.81E-03	7.55E-03	-5.74E-03
962	9.62E-02	0.413	-0.3168	1.52	1.61	-0.09	4.06	4.03	0.03	5.27E-04	3.61E-03	-3.08E-03
944	4.86E-02	0.265	-0.2164	0.144	1.53	-1.386	0.402	4.42	-4.018	1.77E-04	2.09E-03	-1.91E-03
922	5.33E-02	0.175	-0.1217	6.34E-02	0.997	-0.9336	0.148	2.88	-2.732	1.97E-04	1.37E-03	-1.17E-03
896	6.03E-02	0.135	-0.0747	5.06E-02	0.642	-0.5914	9.78E-02	1.89	-1.7922	1.60E-04	8.43E-04	-6.83E-04
865	5.41E-02	0.102	-0.0479	2.76E-02	0.525	-0.4974	4.79E-02	1.6	-1.5521	1.03E-04	5.82E-04	-4.79E-04
831	1.02E-02	9.15E-02	-0.0813	1.90E-02	0.49	-0.471	3.18E-02	1.54	-1.5082	2.97E-05	4.27E-04	-3.97E-04
792	7.41E-04	6.06E-02	-0.059859	7.05E-03	0.393	-0.38595	1.09E-02	1.25	-1.2391	6.00E-06	2.49E-04	-2.43E-04
749	2.72E-05	3.13E-02	-0.031273	1.18E-03	0.217	-0.21582	1.48E-03	0.686	-0.68452	0	1.21E-04	-1.21E-04
701	0	1.31E-02	-0.0131	0	4.20E-02	-0.042	0	0.136	-0.136	0	3.53E-05	-3.5E-05
625	0	2.43E-02	-0.0243	0	2.25E-02	-0.0225	0	0.237	-0.237	0	5.01E-05	-5E-05
<b>Total</b>	<b>159</b>	<b>155</b>	<b>3.72</b>	<b>36.1</b>	<b>32.9</b>	<b>3.2</b>	<b>33.3</b>	<b>29.2</b>	<b>4.1</b>	<b>6.14</b>	<b>6.36</b>	<b>-0.22</b>

**Table 4.** Total domain totals for CO, NO<sub>x</sub>, SO<sub>2</sub>, NH<sub>3</sub>, CH<sub>2</sub>O (formaldehyde), C<sub>5</sub>H<sub>8</sub> (isoprene), and C<sub>2</sub>H<sub>6</sub> for vertical layers.

Pressure (mb)	Formaldehyde (Gg C/day)			Isoprene (Gg C/day)			Ethane (Gg C/day)		
	WRF	CMAQ	WRF-CMAQ	WRF	CMAQ	WRF-CMAQ	WRF	CMAQ	WRF-CMAQ
1011	0.117	0.624	-0.507	0.0124	54.1	-54.1	0.299	1.85	-1.55
1008	3.77E-03	6.08E-03	-2.31E-03	1.33E-04	2.08E-04	-0.0000748	2.38E-02	2.05E-02	3.25E-03
1003	3.77E-03	6.29E-03	-2.52E-03	9.43E-05	2.16E-04	-1.22E-04	5.46E-03	1.83E-02	-1.28E-02
997	3.83E-03	5.78E-03	-1.95E-03	4.64E-05	1.66E-04	-1.20E-04	5.76E-03	1.37E-02	-7.99E-03
989	1.35E-03	4.23E-03	-2.88E-03	3.71E-05	1.04E-04	-6.65E-05	1.02E-03	8.15E-03	-7.13E-03
977	4.78E-04	2.17E-03	-1.69E-03	1.00E-07	6.59E-05	-6.58E-05	3.77E-04	3.30E-03	-2.92E-03
962	6.04E-05	1.01E-03	-9.48E-04	0	2.74E-05	-2.74E-05	1.56E-04	1.18E-03	-1.03E-03
944	2.56E-05	5.78E-04	-5.52E-04	0	1.60E-05	-1.60E-05	2.61E-05	5.95E-04	-5.69E-04
922	3.02E-05	3.89E-04	-3.59E-04	0	1.03E-05	-1.03E-05	1.58E-05	3.50E-04	-3.34E-04
896	2.32E-05	2.72E-04	-2.49E-04	0	8.50E-06	-8.50E-06	1.43E-05	2.24E-04	-2.10E-04
865	1.89E-05	1.83E-04	-1.64E-04	0	5.70E-06	-5.70E-06	1.23E-05	1.62E-04	-1.50E-04
831	1.22E-05	1.18E-04	-1.06E-04	0	3.70E-06	-3.70E-06	1.08E-05	1.35E-04	-1.25E-04
792	2.50E-06	6.34E-05	-6.09E-05	0	2.20E-06	-2.20E-06	3.40E-06	8.49E-05	-8.15E-05
749	0	2.59E-05	-2.59E-05	0	1.10E-06	-1.10E-06	1.00E-07	4.30E-05	-4.29E-05
701	0	6.60E-06	-6.60E-06	0	0	0	0	8.80E-06	-8.80E-06
625	0	7.30E-06	-7.30E-06	0	1.00E-07	-1.00E-07	0	8.90E-06	-8.90E-06
<b>Total</b>	<b>0.131</b>	<b>0.652</b>	<b>-0.521</b>	<b>0.0127</b>	<b>54.1</b>	<b>-54.1</b>	<b>0.336</b>	<b>1.91</b>	<b>-1.58</b>

**Table 4.** Continued

#### 4. Proposed Work

The starting point for the proposed research will be running WRF/Chem over Northeast United States grid for ozone episodes of summer 2002. CMAQ runs for this time period have already been performed within the atmospheric chemistry group for another project and are available for use. Currently WRF/Chem is running based

on meteorological fields from the NCEP Global Forecast System (GFS). The ultimate goal is to run WRF/Chem based on Modern Era Retrospective-analysis for Research and Applications (MERRA) Reanalysis coupled with GMAO GEOS5 assimilation system. MERRA Reanalysis will cover the modern era from 1979 through the present. Unfortunately, MERRA production runs will begin April 2007. In the mean time, GEOS-4 will be used as the meteorological input for WRF/Chem, allowing for an easy transition to GEOS-5/MERRA fields in the future. The first portion of the project will be setting up WRF/Chem to read in GEOS-4 fields and if necessary supplementing some missing variables with fields from GFS.

For the Northeast U.S. WRF/Chem and CMAQ output will be compared for such trace gases as CO, O<sub>3</sub>, SO<sub>2</sub>, and NO<sub>x</sub> based on:

- Total column domain concentrations
- Vertical profiles at selected points such as Baltimore-Washington metro area or major emission sources (i.e. power plants).

Analysis of WRF/Chem performance for the U.S. should allow for any troubleshooting that needs to be done, since more users have ran the model over the U.S. domain than over the China domain. WRF convection evaluation such as the one performed for CMAQ will need to be done to ensure that WRF is capturing convection accurately.

Once proper configuration for the U.S. domain is ensured, WRF/Chem will be set up to use different meteorological and emissions inputs. I will first attempt to configure the model using David Streets 2002 Asian emission inventory described above. Any changes that might have to be implemented in the model to incorporate these or more appropriate data for the region will be performed.

When WRF/Chem is set up for the Northeast and Southeast Asia domain (**Figure 3**), April 2005 runs will be performed for the region of ground and aircraft observations during EAST-AIRE. Ground observations, aircraft data and model output will then be analyzed. The goal is to capture frontal passage within WRF/Chem and to look at the transport and redistribution of pollutants in front of and behind the cold front in comparison with observations. For different test cases, I will investigate the strength of pollutant outflow from East Asia in relationship with vertical transport mechanisms out of the BL (i.e WCB, convection, fronts).

Next I will run simulations of cold surge and convective events over South China Sea (**Figure 3c**) in December 2004 and January 2005 for comparison with 1978-1979 WMONEX ozone concentrations. This portion of the project will be used to quantify the change in average ozone concentrations over the South China Sea during the past two decades. If meteorological data from MERRA Reanalysis will be available, I hope to simulate several cold surge events over the South China Sea in December 1978 and compare model results with WMONEX observations. Modeling December 28 flight, I hope to investigate the mechanisms by which ozone-rich air reached 6 km altitude over the South China Sea, perhaps noting open cell convection.

I will analyze Asian outflow of CO, O<sub>3</sub>, SO<sub>2</sub>, and NO<sub>x</sub>, to the Pacific in the spring by simulating EAST-AIRE and in winter by simulating WMONEX. Analysis of flight and model data will be performed. The passage of a cold front will be defined as the occurrence of increased surface pressure and decreased surface temperature in central eastern China. Several types of plots will be created for analysis: latitudinal and longitudinal distributions of selected species, vertical profiles with respect to latitude/longitude, and vertical profiles with daily mean values in the model corresponding to locations and time of the flight. Analysis criteria will be determined based on each case scenario.

WRF/Chem is a relatively new model still being enhanced and upgraded by the scientific community. Within the WRF community there have been talks about developing a global WRF/Chem model. The current multi-scale WRF/Chem is capable of simulating long range transport of Asian pollution over the Pacific Ocean but is constrained by computational resources on the platform it is installed on. The ultimate goal would be to use WRF/Chem to simulate the proposed episodes and look at the outflow of uplifted pollutants over the Pacific Ocean and ultimately inflow to Western U.S. If this will be feasible, I would be interested in quantifying the effect of Asian pollutant outflow on air quality in Western U.S.

## 5. Summary

Rapid economic growth and industrialization combined with growing population in Eastern Asia is a major focus of environmental studies. Emissions from East Asia are detected locally and thousands of kilometers downwind. Meteorological mechanisms responsible for lofting pollutants from the ground into the free troposphere are the focal point of the current study. Model results combined with ground and aircraft observations will be used to analyze chemical transport in the vicinity of cold fronts. Depending on computational and data resources modeling simulations will be extended to follow Asian pollutant outflow over the Pacific Ocean and study its effects on local air quality in Western United States. The proposed research project will contribute to the scientific community's knowledge of WRF/Chem capabilities and limitations both for regional scale simulations over Eastern Asia and long-range transport simulations over the Pacific Ocean.

## 6. References

- Akimoto, H., and H. Narita (1994), Distribution of SO<sub>2</sub>, NO<sub>x</sub> and CO<sub>2</sub> emissions from fuel combustion and industrial activities in Asia with 1°x1° resolution, *Atmos. Environ.*, 28, 213-225.
- Bethan, S., et al. (1998), Chemical air mass differences near fronts, *J. Geophys. Res.*, 103, 413-434.
- Bey, I., et al. (2001), Asian chemical outflow to the Pacific in spring: Origins, pathways, and budgets, *J. Geophys. Res.*, 106, 23,097- 23,114,.
- Browning, K. A. (1990), Organization of clouds and precipitation in extratropical cyclones, *Extratropicalcyclones: The Erik H. Palmen Memorial Volume, Amer. Meteor. Soc.*, 129-153.
- Chatfield, R. B., and P. J. Crutzen (1984), Sulfur dioxide in remote oceanic air: Cloud transport of reactive precursors, *J. Geophys. Res.*, 89, 7111-7132.
- Cooper, O. R., et al. (2004), A case study of transpacific warm conveyor belt transport: Influence of merging airstreams on trace gas import to North America, *J. Geophys. Res.*, 109.
- Dickerson, R. R., et al. (1987), Thunderstorms: An important mechanism in the transport of air pollutants, *Science*, 235, 460-465.
- Dickerson, R. R., et al. (2006), Aircraft observations of dust and pollutants over NE China: Insight into the meteorological mechanisms of long-range transport, *J. Geophys. Res.*, submitted.
- Ding, Y. (1990), Build-up, air mass transformation and propagation of the Siberian High and its relation to cold surge in East Asia *Meteorol. Atmos. Phys.*, 44, 281- 292.

- Garreaud, R. D. (2001), Subtropical cold surges: Regional aspects and global distribution, *Int. J. Climatol.*, *21*, 1181-1197.
- Grell, G. A., et al. (2000), Application of a multiscale, coupled MM5/chemistry model to the complex terrain of the VOTALP valley campaign, *Atmospheric Environment*, *34*, 1435-1453.
- Harrold, T. W. (1973), Mechanisms influencing the distribution of precipitation within baroclinic disturbances, *Q. J. R. Meteorol. Soc.*, *99*, 232-251.
- Jaffe, D., et al. (2003), Six 'new' episodes of trans-Pacific transport of air pollutants, *Atmospheric Environment*, *37*, 391-404.
- Kley, D., et al. (1996), Observations of near-zero ozone concentrations over the convective Pacific: Effects on air chemistry, *Science*, 230-233.
- Lelieveld, J., and P. J. Crutzen (1994), Role of deep cloud convection in the ozone budget of the troposphere., *Science*, *264*, 1759-1761.
- Li, C., et al. (2006), In-Situ Measurements of Trace Gases and Aerosol Optical Properties at a Rural Site in Northern China during EAST-AIRE 2005, *J. Geophys. Res.*
- Li, Q., et al. (2003), A global three-dimensional model analysis of the atmospheric budgets of HCN and CH<sub>3</sub>CN: Constraints from aircraft and ground measurements, *J. Geophys. Res.*, *108*(D21), 8827.
- Liu, H., et al. (2003), Transport pathways for Asian pollution outflow over the Pacific: Interannual and seasonal variations, *J. Geophys. Res.*, *108*, 8786.
- Mari, C., et al. (2004), Export of Asian pollution during two cold front episodes of the TRACE-P experiment, *J. Geophys. Res.*, *109*.
- Stockwell, W. R., et al. (1990), The second generation regional acid deposition model chemical mechanism for regional air quality modeling, *J. Geophys. Res.*, *95*, 16,343-316,367.
- Stohl, A. (2001), A 1-year Lagrangian ‘‘climatology’’ of airstreams in the Northern Hemisphere troposphere and lowermost stratosphere, *J. Geophys. Res.*, *106*, 7263-7279.
- Streets, D. G., et al. (2003), An inventory of gaseous and primary aerosol emissions in Asia in the year 2000., *J. Geophys. Res.*, *108*, 8809.
- van Aardenne, J. A., et al. (1999), Anthropogenic NO<sub>x</sub> emissions in Asia in the period 1990-2020, *Atmos. Environ.*, *33*, 633-646.
- Wild, O., and H. Akimoto (2001), Intercontinental transport of ozone and its precursors in a three-dimensional global CTM, *J. Geophys. Res.*, *106*, 727,729-727,744.
- Wilks, D. S. (1995), *Statistical Methods in Atmospheric Sciences: An Introduction*, 500 pp., Academic Press.
- Yanai, M., and C. Li (1994), Mechanism of Heating and the Boundary Layer over the Tibetan Plateau, *Monthly Weather Review*, *122*, 305-323.
- Yienger, J. J., et al. (2000), The episodic nature of air pollution transport from Asia to North America, *J. Geophys. Res.*, *105*, 931-926,945.
- Zhang, D., and W. Zheng (2004), Diurnal Cycles of Surface Winds and Temperature as Simulated by Five Boundary Layer Parameterizations, *J. Appl. Meteorol. Atmos. Phys.*, *43*, 157-169.

<sup>1</sup> World Health Organization (<http://www.wpro.who.int/china/sites/ehe/overview.htm>)

<sup>2</sup> Energy Information Organization (<http://www.eia.doe.gov/emeu/cabs/chinaenv.html>)

<sup>3</sup> People & the Plane ([peopleandplanet.net](http://peopleandplanet.net))